Microsolvation of the Water Cation in Argon: I. Ab Initio and Density Functional Calculations of $H_2O^+-Ar_n$ ($n = 0-4$)

Otto Dopfer*

Institut für Physikalische Chemie, Universität Basel, Klingelbergstrasse 80, CH-4056 Basel, Switzerland

Received: July 12, 2000; In Final Form: September 25, 2000

The intermolecular interaction and microsolvation process of the water cation in its $^2B_1$ ground electronic state with up to four Ar ligands are investigated with quantum chemical ab initio and density functional calculations at the unrestricted HF, MP2, and B3LYP levels of theory using a basis set of aug-cc-pVTZ quality. The intermolecular potential energy surface (PES) of the H_2O^+-Ar dimer calculated at the MP2 level features a planar proton (H)-bound H—O—H—Ar global minimum. The slightly translinear ionic hydrogen bond is characterized by a binding energy, $D_0 \sim 2200$ cm^{-1}, an H−Ar separation, $R_e \sim 1.92$ Å, and a bond angle, $\varphi_e \sim 176°$. The p-bound structure, with the Ar atom attached in a T-shaped fashion to the partially filled $2p_y$ orbital of oxygen, is a local minimum with $D_0 \sim 1300$ cm^{-1} and an O−Ar separation, $R_e \sim 2.47$ Å. The attraction in the H-bound structure is dominated by induction forces, whereas charge transfer from Ar to the $2p_y$ orbital of H_2O^+ provides a significant contribution to the stabilization energy of the p-bound isomer. In the most stable structures of $H_2O^+-Ar_n$ ($n = 1-4$) the first two Ar ligands occupy H-bound sites and the next two ligands are located at the p-bound sites leading to geometries with C_s ($n = 1,3$) and C_{2v} symmetry ($n = 2,4$), respectively.

I. Introduction

In the past few years substantial insight into the stepwise microsolvation process of simple AH^+ ions in argon has been obtained by IR spectroscopy and theoretical calculations of isolated AH^+-Ar_n complexes. Examples include OCH^+-Ar_n ($n = 1-13$),[1,2] $N_2H^+-Ar_n$ ($n = 1-13$),[2,3] $SiOH^+-Ar_n$ ($n = 1-10$),[4] $CH_3^+-Ar_n$ ($n = 1-8$),[5] and $NH_4^+-Ar_n$ ($n = 1-7$).[6−8] These systems serve as models for the investigation of ion-ligand forces, which are spectroscopically far less well characterized than the corresponding neutral−neutral interactions.[9−12] Owing to the charge, the interactions in ionic complexes are stronger and three-body effects, mainly arising from nonadditive induction forces, are more important than in neutral complexes. In the accompanying article (henceforth referred to as article II),[13] IR photodissociation spectra of $H_2O^+-Ar_n$ ($n = 1-14$) and partly deuterated species are reported. For the dimer ($n = 1$), spectra at the level of rotational resolution provide detailed information about the intermolecular potential energy surface (PES) near the equilibrium geometry. For the larger clusters ($n = 2-14$), vibrational spectra provide insight into the cluster growth process via the analysis of size-dependent frequency shifts and photofragmentation branching ratios.

In the present work the PES of the H_2O^+-Ar dimer is characterized in detail at several levels of theory (B3LYP, HF, MP2). The results support the interpretation of the experimental data presented in article II,[13] and provide additional information not directly available from the experimental approach. For example, the calculations give insight into regions of the PES not probed by the experiment (e.g., the existence and stability of different isomers, properties of transition states, barriers for internal rotation), the anisotropy of the PES, the degree of H_2O^+ deformation upon complexation, the nature of the interaction as a function of the relative orientation (e.g., the contributions of dispersion, induction, and charge transfer), the frequencies of unobserved vibrations, the shapes of normal coordinates, etc. The PES of H_2O^+-Ar has not been characterized in detail previously. Ab initio calculations for H_2O^+-Ne/Ar at the MP2 level yielded three planar stationary points: the proton (H)-bound structure with a nearly linear H−bond was found to be the global minimum ($R_{H-Ar} \sim 1.93$ Å and $D_e \sim 1600-1950$ cm^{-1} for H_2O^+-Ar), whereas the bridged and oxygen (O)-bound structures are higher-lying transition states (Figure 1).[14] The H_2O^+ cation in its $^2B_1$ electronic ground state has an unpaired electron in the nonbonding, out-of-plane $2p_y$ orbital of oxygen. (The b_1 molecular orbital of H_2O^+ is mainly an atomic $2p_y$ orbital of O.)[15] Hence, it may be expected that the Ar atom can bind to this orbital in a T-shaped fashion, as such a p-bound structure can additionally be stabilized by partial charge transfer from Ar to H_2O^+ (apart from induction forces arising from the interaction of the charge distribution of H_2O^+

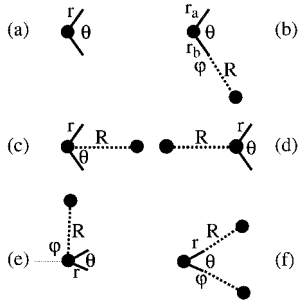

Figure 1. Structures of H_2O^+ (a, C_{2v}), H_2O^+-Ar (b−e), and $H_2O^+-Ar_2$ (f, C_{2v}) calculated at the MP2/aug-cc-pVTZ# level. The H-bound structure is the global minimum of the dimer (b, C_s), the planar bridged (c, C_{2v}) and O-bound structures (d, C_{2v}) are saddle points of first and second order, and the nonplanar p-bound structure (e, C_s) corresponds to a local minimum.

* Corresponding author. E-mail: otto.dopfer@unibas.ch.

10.1021/jp002476a CCC: $19.00
Published on Web 11/21/2000

with the dipole induced on Ar). For CH_3^+-Ar, IR spectroscopy and ab initio calculations showed that, owing to substantial charge transfer from Ar to the vacant $2p_z$ orbital of C, the p-bound structure is the global minimum of this complex and much more stable than the H-bound structure.[5] In H_2O^+-Ar, the unpaired electron in the $2p_y$ orbital somewhat reduces its electrophilic character and the p-bound structure may become energetically comparable with the H-bonded structure which, by comparison with similar H-bound AH^+-Ar dimers, is expected to be stabilized mainly by induction forces.[16,17] Indeed, the present study shows that both structures are minima on the H_2O^+-Ar PES at the MP2 level using relatively large basis sets. The p−bound local minimum of H_2O^+-Ar was not located in the previous MP2 study,[14] because the search for stationary points at the MP2 level was based on the results of gradient optimization at the HF level.

The H_2O^+-Ar dimer constitutes a prototype system for Ar interacting with a bent, triatomic dihydride cation in a doublet electronic state. Comparison with the previously studied closed-shell H_2Cl^+-Ar dimer[18] will reveal the effects of the unpaired electron on the topology of the PES (e.g., interaction strength, anisotropy, internal rotation barriers). In addition, comparison with the neutral H_2O-Ar dimer enables the investigation of the changes in the intermolecular interaction caused by ionization of the molecular subunit. Moreover, because H_2O^+ offers the possibility of forming two H-bonds, the cluster growth in $H_2O^+-Ar_n$ is expected to deviate substantially from that of $AH_k^+-Ar_n$ systems with $k \neq 2$.[1,2,4−6] Differences are expected in the geometry of the first solvation shell, the sequence of shell filling, the presence and stability of isomers, and the magnitude of three-body effects. Magic numbers observed in mass spectra of $H_2O^+-Ar_n$ indicated that the large anisotropy of the H_2O^+-Ar interaction leads to a cluster growth, which is more complicated than in systems with more isotropic ion−Ar interactions.[19] The main focus of the present theoretical study is on the dimer PES, because the experimental data for this cluster size are most extensive.[13] However, theoretical calculations are also desired for the larger cluster sizes, particularly because the vibrational spectra are less informative than the rotationally resolved dimer spectra. Because calculations on larger clusters are only feasible at lower theoretical levels (HF, B3LYP) with the available computer resources, the dimer PES is calculated at both higher (MP2) and lower levels (HF, B3LYP) to investigate the quality of the results obtained at various levels. For example, in AH^+-Ar systems the HF level severely underestimates the interaction strength (roughly by a factor of 2−3 compared with MP2).[5,6] However, the topologies of the PES are often similar at the HF and MP2 levels, so that after appropriate scaling the HF results may be used for reliable interpretation of the experimental data.[5,6] On the other hand, the B3LYP level performs similarly well as MP2 for hydrogen-bonded systems for basis sets of at least triple-ζ quality,[20] whereas it drastically overestimates the interaction for charge transfer.[21] Because the H_2O^+-Ar PES features orientations with H−bonding and charge transfer, the topology of the PES calculated at the B3LYP level is expected to deviate substantially from that calculated at the HF and MP2 levels.

II. Computational Details

Ab initio and density functional calculations for $H_2O^+-Ar_n$ are performed at the unrestricted MP2 ($n = 0-2$), HF ($n = 0-4$), and B3LYP ($n = 0-2$) levels of theory using the GAUSSIAN 94 and GAUSSIAN 98 program packages.[22,23] The aug-cc-pVTZ# basis set used is composed of Ahlrichs VTZ basis functions for the core electrons augmented with diffuse and polarization functions from the aug-cc-pVTZ basis[24] and is similar in quality to the aug-cc-pVTZ basis set.[7] The contraction reads: (13s10p3d2f) → [8s6p3d2f] for Ar, (11s7p3d2f) → [7s4p3d2f] for O, and (6s3p2d) → [4s3p2d] for H. The MP2(full)/aug-cc-pVTZ# level has been shown to yield semi-quantitative intermolecular PES for dimer complexes composed of simple cations and Ar.[7] For computational reasons this level could only be applied to the smaller clusters ($n \leq 2$). The results are used to test the performance of the lower theoretical levels (HF, B3LYP) which can also be applied to the larger cluster sizes. The difference between the HF and MP2 methods provides information of the importance of electron correlation on the intermolecular PES. In all calculations, the spin contamination is negligible ($\langle S^2 \rangle - 0.75 < 0.01$).

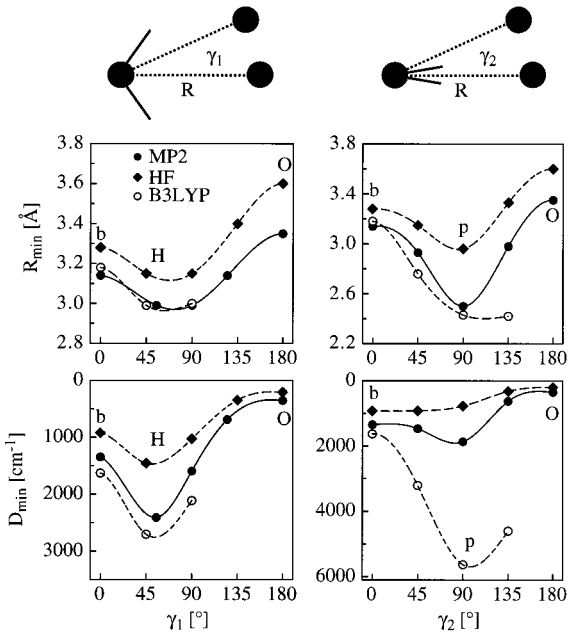

Figure 2. Properties of the intermolecular PES of H_2O^+-Ar calculated at several levels of theory (rigid monomer approximation, aug-cc-pVTZ# basis set). Plotted are the minimal energy separations (R_{min}) and potential energy depths (D_{min}) of 1-D radial cuts through the 3-D PES in (left side) and perpendicular to (right side) the H_2O^+ plane as a function of the angles γ_1 and γ_2. The calculated data points are interpolated by cubic splines. $\gamma_1 \sim 55°$ corresponds to the H-bound global minimum (H), $\gamma_1 = \gamma_2 = 0°$ and $\gamma_1 = \gamma_2 = 180°$ to the bridged (b) and O-bound (O) planar transition states, and $\gamma_2 \sim 90°$ to the p-bound local minimum (p).

All coordinates are relaxed during the search for stationary points. Calculated interaction energies are fully counterpoise-corrected for the basis set superposition error (BSSE).[25] The BSSE corrected energies (E_1) of $H_2O^+-Ar_n$ are further corrected for the relaxation energy (E_2) caused by the complexation-induced deformation of the $H_2O^+-Ar_{n-1}$ fragment, that is, $D_e = E_1 - E_2$.[26,27] The results of the calculations are summarized in Figures 1−4 and Tables 1−11; further details are available upon request. Harmonic vibrational frequencies are scaled by a factor of 0.94256 (MP2), 0.88482 (HF), 0.96592 (B3LYP) to optimize the agreement between calculated and experimental O−H stretching frequencies of H_2O^+ (ν_1 and ν_3). The scaled frequencies are used to approximate the zero-point vibrational energies of stationary points, which are subsequently used to estimate dissociation energies, D_0, from the respective well depths, D_e.

To investigate the three-dimensional (3-D) intermolecular PES in some detail, interaction energies are calculated for a grid of

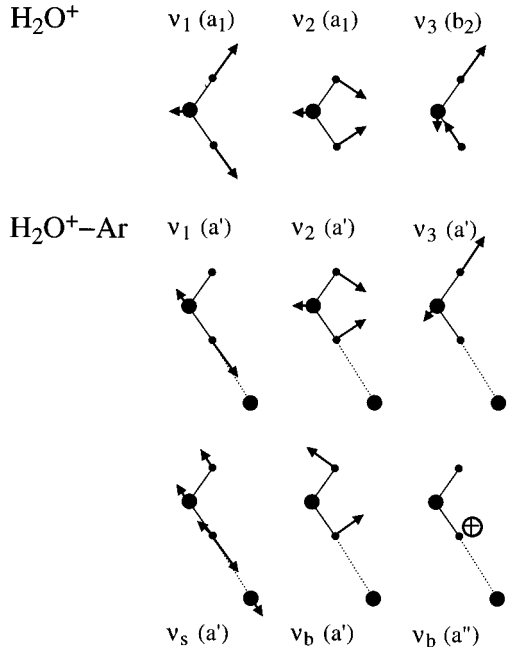

Figure 3. Normal modes of H_2O^+ (C_{2v}) and the H-bound H_2O^+-Ar dimer (C_s) calculated at the MP2/aug-cc-pVTZ# level. Only major displacements are indicated.

intermolecular coordinates, R and γ_i ($i = 1,2$), where γ_i measures the angle between the O—Ar bond (length R) and the C_2 axis of H_2O^+ (Figure 2). In these calculations the structure of H_2O^+ is kept fixed at the optimized monomer geometry (rigid monomer approximation). Only those dimer structures are considered in which the O—Ar bond is lying in one of the two symmetry planes of H_2O^+, corresponding to H_2O^+ internal rotations around its c (angle γ_1) and a (angle γ_2) inertial axes, respectively. The investigated angles are $\gamma_i = 0°$, 45°, 90°, 135°, and 180° ($i = 1,2$) for all theoretical levels (except for MP2, where $\gamma_1 = 45°$ and 135° are replaced by 55° and 125°). For each angle γ_i, the interaction energies of at least 10 radial points spaced by 0.1 Å are least-squares fitted to the analytic expression $V(R) = A \times e^{-BR} - C \times (R - D)^{-4}$: the first term models the exchange repulsion, whereas the second term approximates the charge-induced dipole attraction. Minimum energies, D_{min}, and their corresponding intermolecular separations, R_{min}, of these 1-D radial cuts, $V(R)$, through the 3-D intermolecular PES are plotted in Figure 2 as a function of γ_i ($i = 1,2$). The values for angles intermediate between calculated points are interpolated by cubic splines. Calculations at the B3LYP level yield for $\gamma_1 = 135°$ and 180° radial potential curves without minima (in the range 2.0 Å < R < 6.0 Å), indicating that this level of theory is not even suitable for a qualitative description of this region of the PES.

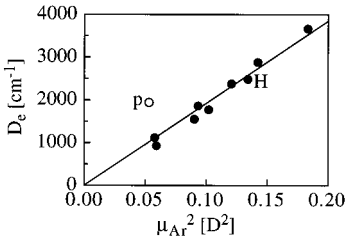

Figure 4. Interaction energies, D_e, of selected H-bound AH^+-Ar dimers (closed circles) calculated at the MP2/aug-cc-pVTZ# level are plotted against the square of the induced dipole moments on Ar, μ_{Ar}^2 (AIM analysis, Table 7). The data point for the p-bound H_2O^+ dimer (open circle) substantially deviates from the linear D_e vs μ_{Ar}^2 relation, indicating the significant stabilization arising from partial charge transfer in this orientation.

III. Results and Discussion

A. Monomer ($n = 0$). The calculated properties of H_2O^+ in the $^2B_1$ electronic ground state (C_{2v} symmetry, Figure 1a) are compared in Tables 1 and 2 with available experimental gas-phase[28−33] and Ne-matrix isolation data[34] and the results of previous ab initio calculations.[14,35−40] As expected, for the aug-cc-pVTZ# basis set used, the MP2 level yields better agreement with the experimental data compared with HF and B3LYP: the structural parameters, bond length r_e and bond angle θ_e (Figure 1a), and fundamental frequencies (after scaling) agree to within 0.001 Å, 0.3°, and 25 cm^{-1} with the values derived from high-resolution spectroscopic studies.[31,32]

B. Dimer ($n = 1$). *1. Potential Energy Surface*. First, the topology of the intermolecular PES calculated at the MP2 level is discussed (Figure 2). The global minimum of this PES corresponds to the planar H-bound H_a—O—H_b^+—Ar structure (Figure 1b, C_s symmetry, $\gamma_1 \sim 55°$). According to gradient optimization the intermolecular bond is characterized by an intermolecular Ar−H_b separation, $R_e = 1.9154$ Å, a bond angle $\varphi_e = 176.1°$ (*trans*-configuration), and dissociation energies, $D_e = 2484.3$ cm^{-1} and $D_0 = 2194.6$ cm^{-1} (Table 3). Complexation with Ar causes a significant deformation of the H_2O^+ monomer structure ($E_2 = 121.5$ cm^{-1}), mainly along the radial coordinates: the free O−H_a bond becomes slightly shorter ($\Delta r_{ae} = -0.0041$ Å), whereas the bound O—H_b bond length increases substantially ($\Delta r_{be} = 0.0289$ Å), an effect typical of hydrogen bonding. In addition, the H—O—H bond angle opens slightly ($\Delta\theta_e = 0.4°$).

The planar bridged structure (Figure 1c, C_{2v} symmetry, $\gamma_1 = \gamma_2 = 0°$) corresponds to the transition state for interconversion of the two equivalent H-bound minima via hydrogen exchange by a rotation of H_2O^+ around its c-axis. The intermolecular bond of this stationary point, is characterized by $R_{O-Ar} = 3.1079$ Å, $R_{H-Ar} = 2.6358$ Å, $D_e = 1373.9$ cm^{-1}, and $D_0 = 1306.4$ cm^{-1} (Table 3). Because the interaction is weaker than in the global

TABLE 1: Equilibrium Structure and Rotational Constants of the H_2O^+ Cation in Its $^2B_1$ Electronic Ground State (C_{2v}, Figure 1a) Calculated at Various Levels of Theory Are Compared with Experimental (exp) Data

method	r_e (Å)	θ_e (°)	A_e (cm^{-1})	B_e (cm^{-1})	C_e (cm^{-1})	refs
MP2/aug-cc-pVTZ#	0.9980	109.6	28.4378	12.5797	8.7216	this work
HF/aug-cc-pVTZ#	0.9804	111.8	31.1451	12.6960	9.0194	this work
B3LYP/aug-cc-pVTZ#	1.0055	109.9	28.2311	12.3458	8.5895	this work
MP2/TZP	0.9998	109.8				14
MP2/6-311G**	0.997	109.1				37
CEPA1	1.005	109.4				35,36
MRCI	1.0004	109.1	27.9561	12.5971	8.6841	38
MRCI	0.9995	109.3				40
exp	1.001	108.9				30
exp	0.9992(6)	109.3(1)	27.789	12.588	8.700	32
exp	1.00(4)	108.4(5)				33

TABLE 2: Calculated Harmonic Vibrational Frequencies (Unscaled and Scaled, cm^{-1}) of the Electronic Ground State of H_2O^+ ($^2B_1$, C_{2v}) and Its Deuterated Isotopomers Compared with Experimental Values[a]

	H_2O^+			HDO^+			D_2O^+			
method	ν_1 (a_1)	ν_2 (a_1)	ν_3 (b_2)	ν_1 (a')	ν_2 (a')	ν_3 (a')	ν_1 (a_1)	ν_2 (a_1)	ν_3 (b_2)	refs
MP2/aug-cc-pVTZ#	3402.1	1468.3	3464.1	2495.5	1287.5	3434.2	2449.4	1076.0	2543.6	this work
	3206.7	*1384.0*	*3265.1*	*2352.1*	*1213.5*	*3236.9*	*2308.6*	*1014.2*	*2397.5*	
	(124)	(172)	(491)	(132)	(130)	(323)	(59)	(68)	(235)	
HF/aug-cc-pVTZ#	3634.8	1532.3	3679.6	2659.8	1343.6	3657.9	2616.8	1123.0	2704.2	this work
	3216.1	*1355.8*	*3255.8*	*2353.4*	*1199.6*	*3236.6*	*2315.4*	*993.7*	*2392.7*	
	(148)	(196)	(557)	(158)	(148)	(366)	(72)	(79)	(269)	
B3LYP/aug-cc-pVTZ#	3327.4	1443.4	3372.9							this work
	3214.0	*1394.2*	*3257.9*							
	(124)	(169)	(457)							
MP2/6-31G**	3460.7	1484.0	3552.3							14
CEPA1	3346	1475	3368							35,36
	3165	*1409*	*3202*							
MRCI	3380.6	1476.6	3436.3	2477.8	1294.7	3409.3	2434.6	1081.8	2522.7	38
	3211.0	*1410.4*	*3255.0*				*2346.2*	*1047.0*	*2424.2*	
MRCI	*3215.87*	*1412.15*	*3261.80*	*2387.9*	*1244.6*	*3238.4*	*2350.7*	*1047.4*		40
exp		*1408.404(30)*								28
exp	*3205(3)*	*1407(3)*					*2342(4)*	*1045(4)*		29
exp		*1408.4153(65)*								31
exp	*3213.00(9)*		*3259.031(3)*							30
exp	*3212.8598(30)*		*3259.0360(20)*							32
exp (Ne matrix)	*3182.7*	*1401.7*	*3219.5*	*2365.6*	*1236.1*	*3199.7*	*2326.7*	*1040.5*	*2392.7*	34
					1245.7	*3202.9*				

[a] Fundamental frequencies are listed in italics. Calculated IR intensities (km/mol) are given in parentheses.

TABLE 3: Calculated Structures (Å), Rotational Constants, and Energies (cm^{-1}) of Several Stationary Points on the Potential Energy Surface of the Electronic Ground State of H_2O^+−Ar

structure	method	nature[a]	r_e (r_{ae}/r_{be})	θ_e/φ_e (°)	R_e	A_e	B_e	C_e	E_1	E_2	D_e/D_0
H-bound	MP2/aug-cc-pVTZ#	GM	0.9939/1.0269	110.0/176.1	1.9154	21.465	0.1591	0.1579	2605.8	121.5	2484.3/2194.6
($^2A''/C_s$)	HF/aug-cc-pVTZ#	GM	0.9775/0.9929	111.8/177.8	2.1213	22.422	0.1417	0.1409	1599.1	31.0	1568.1/1320.3
	B3LYP/aug-cc-pVTZ#	LM	0.9995/1.0393	110.2/175.9	1.9116	21.326	0.1581	0.1570	3287.3	173.8	3113.5/2972.0
	MP2/TZP[b]	GM	0.9959/1.0234	109.8/−	1.9265						
p-bound	MP2/aug-cc-pVTZ#	LM	0.9922	108.6/91.8	2.4657	8.8322	0.2218	0.2198	1969.6	30.9	1938.7/1309.5
($^2A'/C_s$)	HF/aug-cc-pVTZ#	*c*									
	B3LYP/aug-cc-pVTZ#	GM	0.9883	108.1/78.2	2.3888	9.0601	0.2332	0.2309	6056.7	136.3	5920.4/5015.3
O-bound	MP2/aug-cc-pVTZ#	SP2	0.9979	109.5	3.2877	12.597	0.1203	0.1192	394.5	0.1	394.4/360.5
($^2B_1/C_{2v}$)	HF/aug-cc-pVTZ#	SP2	0.9804	111.8	3.6300	12.696	0.0993	0.0986	275.7	8.2	267.5/249.4
	B3LYP/aug-cc-pVTZ#	*c*									
bridged	MP2/aug-cc-pVTZ#	SP1	0.9991	106.6	3.1079	13.026	0.1460	0.1444	1412.0	38.1	1373.9/1306.4
($^2B_1/C_{2v}$)	HF/aug-cc-pVTZ#	SP1	0.9803	110.1	3.2767	12.956	0.1309	0.1296	1015.5	21.6	993.9/907.8
	B3LYP/aug-cc-pVTZ#	SP2	1.0017	107.2	3.1517	12.871	0.1419	0.1403	1843.1	46.8	1796.3/1747.2

[a] GM, global minimum; LM, local minimum; SP*n*, *n*th order stationary point featuring *n* imaginary frequencies. [b] Ref 14. [c] Efforts in locating stationary points failed.

H-bound minimum, the complexation-induced deformation of H_2O^+ is smaller ($E_2 = 38.1$ cm^{-1}): the double hydrogen bond leads to modest elongations of the O—H bonds ($\Delta r_e = 0.0011$ Å) and a reduction in the bond angle ($\Delta\theta_e = -3°$). The two equivalent H-bound minima can also be connected by a rotation of H_2O^+ around its *c*-axis via the planar O-bound structure (Figure 1d, C_{2v} symmetry, $\gamma_1 = \gamma_2 = 180°$). The intermolecular bond is very weak in this configuration ($R_e = 3.2877$ Å, $D_e = 394.4$ cm^{-1}, $D_0 = 360.5$ cm^{-1}) and causes only minor perturbations of H_2O^+ ($E_2 = 0.1$ cm^{-1}, $\Delta r_e = -0.0001$ Å, $\Delta\theta_e = -0.1°$). Following the minimum energy path along the rotation of H_2O^+ around its *a*-axis (Figure 2), the bridged and O-bound geometries are connected via a local minimum on the PES, where the Ar atom is attached in a T-shaped fashion to the $2p_y$ orbital of O (Figure 1e, C_s symmetry, $\gamma_2 \sim 90°$). The intermolecular bond of this p-bound structure is described by $R_{O-Ar} = 2.4657$ Å, $R_{H-Ar} = 2.6405$ Å, $\varphi_e = 91.8°$, $D_e = 1938.7$ cm^{-1}, and $D_0 = 1309.5$ cm^{-1} (Table 3). The significant energy difference in the potential between the bridged and p-bound structures, $\Delta D_e = 564.8$ cm^{-1}, nearly vanishes when the zero-point energies are taken into account, $\Delta D_0 < 5$ cm^{-1}. It is thus not obvious whether a p-bound isomer can be observed experimentally (in addition to the H-bound structure). For the p-bound geometry the effects of Ar complexation on the H_2O^+ structure are $E_2 = 30.9$ cm^{-1}, $\Delta r_e = -0.0058$ Å, and $\Delta\theta_e = -1°$ (Table 3).

Inspection of Figure 2 reveals that the intermolecular PES calculated at the HF level has a topology similar to the MP2 potential. The major difference is that at the HF level the interaction strengths are lower by 40−60% and the bond lengths are longer by 0.15−0.45 Å (depending on the dimer configuration). In addition, the HF potential does not feature a pronounced local minimum at the p-bound configuration (in contrast to the MP2 PES) and the surface is very flat along the γ_2 coordinate near $\gamma_2 = 90°$. In fact, efforts to locate a stationary point in this region of the PES by gradient optimization failed at the HF level. In general, the perturbation of the H_2O^+ monomer at the HF level is smaller than at the MP2 level, owing to the weaker intermolecular interaction. As expected,[20] the topology of the PES calculated at the B3LYP level is similar to the MP2 surface in regions where the Ar atom is close to a proton, that is, for configurations with hydrogen bonding (γ_1

TABLE 4: Calculated Scaled Harmonic Frequencies (cm^{-1}) and IR Intensities (km/mol, in Parentheses) of Several Stationary Points on the Potential Energy Surface of the Electronic Ground State of H_2O^+-Ar

structure	method	nature[a]	ν_1	ν_2	ν_3	ν_s	ν_b	ν_b
H-bound ($^2A''/C_s$)	MP2/aug-cc-pVTZ#	GM	2730.1 (a′/1598)	1381.4 (a′/96)	3282.0 (a′/313)	207.4 (a′/78)	352.4 (a′/122)	481.9 (a″/119)
	HF/aug-cc-pVTZ#	GM	2991.9 (a′/1114)	1359.2 (a′/138)	3269.7 (a′/370)	137.0 (a′/63)	245.7 (a′/122)	319.9 (a″/157)
	B3LYP/aug-cc-pVTZ#	LM	2587.3 (a′/894)	1382.2 (a′/97)	3297.9 (a′/350)	215.0 (a′/66)	352.1 (a′/112)	314.6 (a″/123)
	exp[b]		2672	∼1384	3283.9	200		
p-bound ($^2A'/C_s$)	MP2/aug-cc-pVTZ#	LM	3254.5 (a′/186)	1412.0 (a′/135)	3334.0 (a′/399)	149.1 (a′/72)	556.8 (a′/321)	407.8 (a″/3)
	HF/aug-cc-pVTZ#	*c*						
	B3LYP/aug-cc-pVTZ#	GM	3365.7 (a′/420)	1459.7 (a′/118)	3458.7 (a′/310)	252.5 (a′/37)	629.1 (a′/180)	510.7 (a″/0)
O-bound ($^2B_1/C_{2v}$)	MP2/aug-cc-pVTZ#	SP2	3206.8 (a_1/138)	1384.4 (a_1/171)	3266.5 (b_2/473)	66.0 (a_1/42)	111.2 *i* (b_2/94)	183.5 *i* (b_1/353)
	HF/aug-cc-pVTZ#	SP2	3216.1 (a_1/164)	1355.5 (a_1/199)	3256.6 (b_2/542)	35.8 (a_1/41)	44.9 *i* (b_2/100)	104.9 *i* (b_1/392)
	B3LYP/aug-cc-pVTZ#	*c*						
bridged ($^2B_1/C_{2v}$)	MP2/aug-cc-pVTZ#	SP1	3204.1 (a_1/159)	1380.5 (a_1/325)	3236.8 (b_2/358)	127.5 (a_1/55)	278.9 *i* (b_2/162)	41.9 (b_1/365)
	HF/aug-cc-pVTZ#	SP1	3222.2 (a_1/171)	1360.8 (a_1/311)	3248.9 (b_2/450)	91.6 (a_1/51)	174.4 *i* (b_2/156)	76.4 (b_1/401)
	B3LYP/aug-cc-pVTZ#	SP2	3179.1 (a_1/505)	1396.8 (a_1/89)	3286.0 (b_2/305)	102.4 (a_1/21)	270.8 *i* (b_2/154)	604.5 *i* (b_1/431)

Available experimental values are listed for comparison. [a] GM, global minimum; LM, local minimum; SP*n*, *n*th order stationary point featuring *n* imaginary frequencies. [b] Ref 13. [c] Efforts in finding stationary points failed.

TABLE 5: Scaled Harmonic Frequencies (cm^{-1}), IR Intensities (km/mol, in Parentheses), and Dissociation Energies (cm^{-1}) of Several Isotopomeric Structures of H-bound H_2O^+-Ar (C_s) Calculated at the MP2/aug-cc-pVTZ# Level

structure		ν_1 (a′)	ν_2 (a′)	ν_3 (a′)	ν_s (a′)	ν_b (a′)	ν_b (a″)	D_0
Ar−HOH^+	calc	2730.1 (1598)	1381.4 (96)	3282.0 (313)	207.4 (78)	352.4 (122)	481.9 (119)	2194.6
	exp[a]	2672	∼1384	3283.9	200			
Ar−HOD^+	calc	2730.9 (1646)	1244.9 (69)	2368.6 (114)	204.0 (85)	286.8 (54)	481.6 (127)	2227.2
	exp[a]	2689			194			
Ar−DOH^+	calc	1990.4 (777)	1182.2 (82)	3281.6 (315)	203.0 (71)	295.1 (86)	345.4 (50)	2236.7
	exp[a]			3286.7				
Ar−DOD^+		1988.4 (758)	1009.4 (34)	2388.9 (179)	200.0 (81)	252.8 (40)	345.1 (58)	2252.2

Available experimental values are given for comparison. [a] Ref 13.

TABLE 6: Results of the AIM Population Analysis (Charge Distribution and Induced Dipole Moment) in H_2O^+ and Various H_2O^+-Ar Dimer Structures Calculated at the MP2/aug-cc-pVTZ# Level

structure	$q(H_a)$ (e)	$q(H_b)$ (e)	$q(O)$ (e)	$q(Ar)$ (e)	$\mu(Ar)$ (D)
H_2O^+	0.76	0.76	−0.53		
H-bound H_2O^+-Ar	0.75	0.74	−0.55	0.06	0.37
p-bound H_2O^+-Ar	0.75	0.75	−0.61	0.11	0.23
O-bound H_2O^+-Ar	0.76	0.76	−0.53	0.01	0.16

$= 0-90°$, $\gamma_2 = 0°$). However, the intermolecular interaction is greatly overestimated in the region of the p-bound geometry ($\gamma_2 \sim 90°$), for which the binding energy at the B3LYP level is more than three times greater than at the MP2 level (D_e = 5920.4 vs 1938.7 cm^{-1}, D_0 = 5015.3 vs 1309.5 cm^{-1}, Table 3). Consequently, at the B3LYP level the p-bound geometry is much lower in energy than the H-bound structure, in contrast to the HF and MP2 surfaces and the experimental evidence (article II).[13] In addition, for structures with $\gamma_i > 135°$ the radial cuts calculated at the B3LYP level decrease monotonically between 2 and 6 Å, suggesting that this level provides only a realistic approximation of the PES in the region of hydrogen bonding. In this region, the interaction is slightly stronger than for the MP2 surface, leading to larger perturbations of H_2O^+ upon Ar complexation (Table 3).

To elucidate the nature of the intermolecular bond, the charge distribution in H_2O^+ and several H_2O^+-Ar dimer structures is determined using the atoms-in-molecules (AIM) and Mulliken (MUL) population analyses. The results do not depend strongly on the theoretical level (HF, B3LYP, MP2), but on the method chosen for the population analysis. For example, the AIM charges in H_2O^+ are $q_H = 0.76\ e$ and $q_O = -0.53\ e$, whereas the MUL charges are $q_H = 0.29\ e$ and $q_O = 0.42\ e$ (at the MP2 level). Because the AIM analysis is more reliable than the MUL analysis,[41] the MUL charge distributions are not discussed further. According to the AIM analysis at the MP2 level (Table 6), there is almost no charge rearrangement upon complexation for the O-bound H_2O^+-Ar dimer. For the H-bound dimer only little charge is transferred from Ar to H_2O^+ ($q_{Ar} = 0.06\ e$), indicating that induction forces dominate the attraction in this dimer orientation. The charge distribution in H_2O^+ induces a dipole moment of $\mu_{Ar} = 0.37$ D on Ar. For the p-bound dimer, the charge transfer is larger ($q_{Ar} = 0.11\ e$), whereas induction is weaker ($\mu_{Ar} = 0.23$ D). Thus, it can be concluded that in the H-bound structure the attraction is dominated by the charge-induced dipole interaction, whereas significant charge transfer from Ar into the electrophilic $2p_y$ orbital of O is involved in stabilizing the p-bound structure. The partial charge transfer in the p-bound structure also explains why the B3LYP level greatly overestimates the interaction in this part of the PES.[21]

TABLE 7: Interaction Energies and Induced Dipole Moments on Ar (AIM Analysis) in Proton-bound AH^+-Ar Dimers Calculated at the MP2/aug-cc−pVTZ# Level

AH^+-Ar	μ_{Ar} (D)	D_e (cm^{-1})	ref
NH_4^+-Ar	0.243	927	7
$SiOH^+-Ar$	0.240	1117	2
OCH^+-Ar	0.300	1551	2
HNH^+-Ar	0.319	1773	16
$HClH^+-Ar$	0.305	1860	18
$OCOH^+-Ar$	0.347	2379	17
HOH^+-Ar	0.366	2484	this work
N_2H^+-Ar	0.377	2881	2
OH^+-Ar	0.428	3666	this work

To illustrate that in H-bound AH^+-Ar dimers induction is the dominant attractive force, the calculated interaction energies of several dimers are plotted as a function of μ_{Ar}^2 in Figure 4 (Table 7). The electric field of the charge distribution in AH^+, *E*, induces a dipole moment on Ar, $\mu_{Ar} = \alpha_{Ar} \times E$ (α_{Ar} is the polarizability of Ar). The energy of μ_{Ar} in the field *E*, $U = -\mu_{Ar} \times E = -\mu_{Ar}^2/\alpha_{Ar}$, is proportional to μ_{Ar}^2. The calculated binding energies of the considered H-bound AH^+-Ar dimers

in Figure 4 reproduce this relation, confirming that in these complexes (with binding energies ranging from 1000 to 4000 cm^{-1}) indeed induction forces provide the dominant contribution to the attractive part of the potential. The data point for the p-bound H_2O^+-Ar structure (open circle) significantly deviates from the linear D_e vs μ_{Ar}^2 relation for the H-bound dimers (closed circles) and the magnitude of the deviation suggests that partial charge transfer increases the binding energy of this dimer by approximately a factor of 2.

Previous calculations at the MP2/TZP and higher levels are in good agreement with the present MP2/aug-cc-pVTZ# results for the geometry and interaction strength of the H-bound global minimum (R_e = 1.9265 Å, $D_e \sim 1600-1950$ cm^{-1}) and the structural changes of H_2O^+ upon complexation (Tables 1 and 3).[14] Moreover, the O-bound and bridged structures were identified as stationary points in ref 14, however, no details were presented. In contrast to the present work, the p-bound local minimum was not identified previously,[14] because the search for stationary points was conducted at the HF level, for which the PES has no local minimum at the p-bound geometry (Figure 2).

2. Normal Modes. Figure 3 compares the normal coordinates of H_2O^+ with those of the H-bound H_2O^+-Ar dimer calculated at the MP2 level. Although some vibrational frequencies depend strongly on the theoretical level (Table 4), the general shape of the normal modes does not. The intramolecular modes are considered first. In free H_2O^+, both O—H bonds are equivalent and the resonant interaction between the two identical local O—H oscillators gives rise to the symmetric and antisymmetric O—H stretch normal modes, ν_1 and ν_3. Complexation with Ar destabilizes the bound O—H_b bond with respect to the free O—H_a bond, thereby destroying this resonance. As a consequence, the O—H stretch modes of H-bound H_2O^+-Ar are nearly pure elongations of the bound and free O—H bonds, respectively. Analysis of the phases of the two O—H oscillators suggests that the bound and free O—H stretch modes of the dimer correlate with the symmetric and antisymmetric stretch modes of the monomer, respectively. Whereas ν_1 experiences a large red shift upon complexation, ν_3 exhibits a small blue shift, in line with the changes in the corresponding O—H bond lengths. The large red shift of ν_1 is accompanied by a strong enhancement of its IR intensity. These observations are typical for hydrogen bonding, and the magnitude of the effects induced by complexation depend strongly on the strength of the intermolecular interaction.[17,42,43] At the MP2 level the binding energy of D_0 = 2194.6 cm^{-1} leads to $\Delta\nu_1 = -476.6$ cm^{-1}, $\Delta\nu_3$ = 16.9 cm^{-1}, and $\Delta I(\nu_1)$ = 1189%. At the HF level the interaction is weaker (D_0 = 1320.3 cm^{-1}, $\Delta\nu_1 = -224.2$ cm^{-1}, $\Delta\nu_3$ = 13.9 cm^{-1}, $\Delta I(\nu_1)$ = 653%), whereas at the B3LYP level it is stronger (D_0 = 2972.0 cm^{-1}, $\Delta\nu_1 = -626.7$ cm^{-1}, $\Delta\nu_3$ = 40.0 cm^{-1}, $\Delta I(\nu_1)$ = 621%). The H_2O^+ bending mode is nearly unaffected upon complexation (Figure 3), and the calculated frequency shifts are $\leq$ 12 cm^{-1} at all three investigated levels.

Because both O—H bonds are equivalent in the bridged, O-bound, and p-bound H_2O^+-Ar structures (Figure 1c—e), the properties of the intramolecular normal coordinates of H_2O^+ (shape, frequency, and intensity) are much less affected by complexation than those of the H-bound global minimum (Table 4). In particular, the O—H stretch normal modes are symmetric and antisymmetric combinations of the two local O—H oscillators. Because of the weak interaction, the frequency shifts are small for the O-bound structure ($|\Delta\nu_i| < 2$ cm^{-1}, MP2 level). For the more strongly bound bridged geometry, the frequency shifts are larger ($|\Delta\nu_i| < 30$ cm^{-1}). Both the H_2O^+ bending and stretching potentials become stiffer upon Ar complexation at the $2p_y$ orbital of H_2O^+, leading to an increase of all frequencies: $\Delta\nu_1$ = 47.8, $\Delta\nu_2$ = 28.0, $\Delta\nu_3$ = 68.9 cm^{-1}. This observation supports the conclusion of partial charge transfer from Ar into the $2p_y$ orbital of H_2O^+, because both the bending and stretching frequencies in the electronic ground state of neutral H_2O are significantly higher than those of H_2O^+ (Table 2 and ref 44).

The three intermolecular modes of the H-bound H_2O^+-Ar dimer are the stretching mode (ν_s) and the two bending modes (ν_b) with a′ (in-plane) and a″ (out-of-plane) symmetry (Figure 3). The latter modes arise from hindered internal rotations of H_2O^+ and have higher frequencies than ν_s, because mainly the light protons are moving and the potential features large angular anisotropy near the H-bound minimum (Figure 2). As expected, the calculated stretching frequencies correlate with the interaction strengths: ν_s = 207.4, 137.0, and 215.0 cm^{-1} and D_e = 2484, 1568, and 3114 cm^{-1} at the MP2, HF, and B3LYP levels. All frequencies are real and positive at all theoretical levels (Table 4), confirming that the H-bound structure is indeed a minimum on the PES.

According to the harmonic frequency analysis, the p-bound structure is a minimum of the PES at the MP2 and B3LYP levels. However, when zero-point corrections are taken into account, the energies of the bridged and p-bound geometries become similar (at MP2), indicating that the corrected potential may be quite flat along the γ_2 coordinate. In addition, no stationary p-bound structure is found at the HF level. As pointed out earlier, the B3LYP level only provides a good description of the PES close to hydrogen bonding. Thus, higher-level calculations are required to ascertain whether the p-bound isomer can be observed experimentally. In the experimental spectrum presented in article II only the H-bound structure has been identified.[13] The O-bound planar structure has imaginary frequencies for both the in-plane and out-of-plane bending modes (at HF and MP2), indicating that the interaction becomes more favorable for Ar by moving toward either the H-bound or p-bound structures. The large imaginary ν_b frequency with b_2 symmetry confirms that the bridged structure is a transition state connecting the two H-bound minima via internal H_2O^+ rotation around its *c*-axis (at all levels). In contrast, the frequency of ν_b with b_1 symmetry is small at the HF and MP2 level, indicating that the PES is flat along the γ_2 angle near $\gamma_2 \sim 0°$ (H_2O^+ rotation around its *a*-axis). At the B3LYP level, the corresponding frequency is large and imaginary, owing to the artificially deep minimum at the p-bound structure.

Table 5 compares the frequencies, IR intensities, and dissociation energies of successively deuterated H/D-bound H_2O^+-Ar dimers calculated at the MP2 level. As expected, the frequencies and IR intensities decrease with the increasing degree of deuteration, whereas the dissociation energies increase. Moreover, for the monodeuterated species, two isomers exist and have been observed experimentally[13]: the H-bound and D-bound dimers D—O—H^+—Ar and H—O—D^+—Ar. Both species have similar binding energies and can be distinguished by their rather different vibrational frequencies. As both O—H stretching modes in H—bound H_2O^+-Ar are localized O—H oscillators, their frequencies drop roughly by a factor $\sqrt{2}$ upon deuteration. The same is true for the ν_b mode with a″ symmetry (Figure 3). In contrast, ν_s is relatively insensitive to deuteration, because the changes in the reduced mass are small for this vibration. As the ν_2 and ν_b(a′) modes involve the motion of both protons, subsequent deuteration has a similar effect for

TABLE 8: Equilibrium Properties of Several HAH^+-Ar Dimers Calculated at the MP2/aug-cc−pVTZ# Level

HAH^+-Ar	φ_e (°)	R_e (Å)	D_e (cm^{-1})	Δr_{be} (Å)	Δr_{ae} (Å)	$\Delta\nu_1$ (cm^{-1})	E_2 (cm^{-1})
HOH^+-Ar	176.1	1.92	2484	0.029	−0.0041	−477	121.5
$HClH^+-Ar$[a]	178.3	1.97	1860	0.031	−0.0037	−407	99.7
HNH^+-Ar[b]	179.8	2.02	1773	0.025	−0.002	−274	45.0

[a] Ref 18. In $HClH^+-Ar$, the bound Cl—H stretch is denoted ν_3. [b] Ref 16.

each step ($\sim 2^{1/4}$) and the frequencies are reduced by $\sim\sqrt{2}$ from H_2O^+-Ar to D_2O^+-Ar.

The comparison between experimental[13] and calculated frequencies for H_2O^+-Ar (Table 4) shows unambiguously that the observed dimer has a H-bound structure. The agreement is semiquantitative for the MP2 and B3LYP levels which indicates that both levels provide a reliable description of the interaction in the H-bound H_2O^+-Ar dimer.[20] These conclusions are also supported by the good agreement between predicted and observed frequency shifts upon deuteration (Table 5). The HF level severely underestimates the interaction strength and predicts far too small values for ν_s and $\Delta\nu_1$, similar to previous calculations at the MP2/6−31G** level.[14] The spectra show no evidence for a p-bound dimer,[13] which is predicted to be the global minimum at the B3LYP level. It may be argued that such a strongly bound p-bound isomer would not be observed in the photodissociation spectrum, as the high binding energy predicted at the B3LYP level ($\sim$5000 cm^{-1}) exceeds the photon energy used. However, this scenario is unlikely as, similar to H_2O^+-Ar, the spectra of H_2O^+-He and H_2O^+-Ne also do not show any signature of p-bound structures, although the B3LYP level predicts p−bound global minima for these dimers.[45] However, these complexes have binding energies well below the photon energies used, that is, the p-bound structures should be visible in the respective photodissociation spectra if they were global minima. Consequently, it is concluded that the B3LYP level severely overestimates the interaction in regions of the potential away from H-bonding, probably owing to an inadequate description of the interaction of Ar with the partially filled $2p_y$ orbital of oxygen (leading to partial charge transfer).[21]

3. Comparison to Related Systems. Table 8 compares the properties of three related HAH^+-Ar dimers (A = O, Cl, N) calculated at the MP2/aug-cc-pVTZ# level.[16,18] The PES of all three complexes feature H-bound global minima with near-linear intermolecular proton bonds. The interaction increases in the order $HNH^+-Ar < HClH^+-Ar < HOH^+-Ar$. In general, the stronger the interaction (D_e), the shorter the intermolecular H—Ar bond (R_e) and the larger its deviation from linearity (180° − φ_e). Moreover, the stronger the intermolecular bond, the larger the perturbation of the monomer properties: this trend is visible in the substantial elongations of the bound A—H bonds (Δr_{be}), the much smaller contractions of the free A—H bonds (Δr_{ae}), the large red shifts in the bound A—H stretching fundamentals ($\Delta\nu_1$), and the monomer deformation energies (E_2).

Previous experimental and theoretical studies revealed that the strength of the intermolecular interaction in closed-shell AH^+-Rg dimers (Rg = He,Ne,Ar) is related to the difference in the proton affinities (PAs) of the two bases A and Rg. For example, for a given base A (e.g., A = CO, CO_2, SiO) the ν_1 red shift is proportional to PA_{Rg}.[12,17,43] On the other hand, for the same Rg atom the interaction is weaker for bases A with higher PA_A.[12,17,43] This rule seems to hold for simple closed-shell AH^+ ions (e.g., $AH^+ = N_2H^+$, $OCOH^+$, OCH^+, $SiOH^+$, NH_4^+) and AH^+ ions with triplet electronic ground states ($AH^+ = OH^+$, HNH^+, O_2H^+),[16,46,47] indicating that the diradical character does not lead to the formation of an incipient chemical bond.[12,16,48,49] However, this rule seems not to be valid for the H_2O^+ ion in its $^2B_1$ electronic ground state. For example, though the PAs of OH and CO are almost identical (PA_{OH} = 593 kJ/mol, PA_{CO} = 594 kJ/mol),[50] the binding energies of HOH^+-Ar and OCH^+-Ar are drastically different (D_e = 2484 vs 1551 cm^{-1}).[2] In addition, the interaction in the closed-shell $HClH^+-Ar$ ion[18] is weaker than in HOH^+-Ar (D_e = 1860 and 2484 cm^{-1}), although the PA of HCl is lower than that of OH (PA_{HCl} = 557 kJ/mol).[50] Because the closed-shell $HClH^+-Ar$ ion obeys the rule,[18] it is probably the radical character of the doublet electronic state of H_2O^+ that causes the H_2O^+-Ar dimer to deviate from the common trend observed for closed-shell and diradical species. From Figure 4 it is evident that the attraction in the H-bound H_2O^+-Ar dimer is dominated by induction, implying that the unpaired electron in the $2p_y$ orbital does not provide additional covalent contributions to the proton bond. Thus, it is concluded that the rather different charge distributions in H_2O^+ ($q_O = -0.53\ e$, $q_H = 0.76\ e$) and H_2Cl^+ ($q_{Cl} = 0.07\ e$, $q_H = 0.46\ e$) are responsible for the larger interaction strength in H_2O^+-Ar than in H_2Cl^+-Ar.[18] Hence, it is suggested that for AH^+ ions with doublet electronic states a separate relation is required to estimate the binding energies of AH^+-Rg dimers from the PA of the base A. To establish such a relation, theoretical and experimental data for other AH^+-Rg radical systems are required (e.g., H_2S^+-Rg).

TABLE 9: Calculated Equilibrium Structure (Å) and Binding Energies (cm^{-1}) of the $H_2O^+-Ar_2$ Trimer (C_{2v}, Figure 1f)

method[a]	r_e	θ_e/φ_e (°)	R_e	E_1	E_2	D_e/D_0
MP2	1.0161	110.3/176.6	1.9676	2162.3	95.7	2066.6/1824.5
HF	0.9877	112.0/177.5	2.1276	1423.9	67.9	1356.0/1175.6
B3LYP	1.0259	110.5/175.3	1.9772	2737.9	154.0	2583.9/2292.6

[a] All calculations use the aug-cc-pVTZ# basis set.

The unpaired electron in the $2p_y$ orbital of H_2O^+ causes the topology and anisotropy of the PES of H_2O^+-Ar (Figure 2) to be largely different from the corresponding PES of the related closed-shell H_2Cl^+-Ar dimer.[18] Both PES have deep H-bound global minima with large barriers for internal rotation. However, whereas the H_2O^+-Ar PES features a local p-bound minimum, which is stabilized by partial charge transfer from Ar to the $2p_y$ orbital of O, the intermolecular interaction in H_2Cl^+-Ar is particularly weak for this orientation, probably owing to substantial exchange repulsion of the filled out-of-plane 3p orbital of Cl (H_2Cl^+ is isoelectronic with H_2S, which is isovalent to H_2O).[18]

Comparison between cationic H_2O^+-Ar and neutral H_2O-Ar reveals the changes in the intermolecular PES upon ionization of H_2O. Similar to H_2O^+-Ar, the calculated PES of H_2O-Ar features a planar, H-bonded global minimum[51] (in good agreement with the potential derived from spectroscopic data[52]). However, the intermolecular bond is much weaker and longer in the neutral dimer ($R_{O-Ar} \sim 3.6$ Å, $D_e \sim 130$ cm^{-1}) and mainly based on dispersion forces. In addition, barriers for in-plane rotation via the bridged and O-bound transition states are very small (23 and 27 cm^{-1}). In contrast to H_2O^+-Ar, the p-bound structure is not a local minimum on the PES of neutral H_2O-Ar, but a transition state for out-of-plane internal rotation with

TABLE 10: Scaled Vibrational Frequencies (cm^{-1}) and IR Intensities (km/mol, in Parentheses) of Several Isotopomeric $H_2O^+-Ar_2$ Trimers

structure	method[a]	ν_1 (a_1/a')	ν_2 (a_1/a')	ν_3 (b_2/a')	ν_b (a_1/a')	ν_s (a_1/a')	ν_s (b_2/a')	ν_b (b_1/a'')	ν_b (a_2/a'')	ν_b (b_2/a')
$Ar-HOH^+-Ar$ (C_{2v})	MP2	2903.4 (515)	1381.9 (61)	2855.0 (2384)	35.5 (5)	165.5 (31)	207.5 (93)	435.4 (250)	456.4 (0)	479.5 (102)
	B3LYP	2819.9 (313)	1379.1 (57)	2778.9 (2161)	36.6 (4)	163.8 (26)	207.9 (98)	308.3 (245)	321.6 (0)	470.4 (100)
	exp[b]	2875		2821						
$Ar-HOD^+-Ar$ (C_s)	B3LYP	2041.4 (608)	1215.2 (47)	2798.5 (1233)	36.4 (4)	161.4 (25)	204.1 (96)	228.0 (65)	313.7 (119)	385.3 (57)
	exp[b]			2844						
$Ar-DOD^+-Ar$ (C_{2v})	B3LYP	2033.2 (151)	1006.3 (19)	2048.5 (1056)	36.1 (4)	159.4 (23)	200.6 (93)	224.7 (91)	228.3 (28)	335.0 (38)

Available experimental values are given for comparison. [a] All calculations use the aug-cc-pVTZ# basis set. [b] Ref 13.

TABLE 11: Bond Lengths (Å), Vibrational Frequencies, and Binding Energies (cm^{-1}) of $H_2O^+-Ar_n$ Calculated at the HF/aug-cc-pVTZ# Level[a]

n	r_e (r_{ae}/r_{be})	R_e(H−Ar)	R_e(O−Ar)	ν_1	ν_3	ν_s(H−Ar)	D_e[b]
0 (C_{2v})	0.9804			3216.1 (148)	3255.8 (557)		
1 (C_s)	0.9775/0.9929	2.1213		2991.9 (1114)	3269.7 (370)	137.0	1568.1
2 (C_{2v})	0.9877	2.1676		3076.7 (392)	3060.8 (1717)	109.6/139.6	1356.0
3 (C_s)	0.9860	2.1942	3.1064	3100.7(341)	3091.8 (1536)	104.8/132.8	572.6
4 (C_{2v})	0.9848	2.2148	3.1304	3116.6 (295)	3113.1 (1422)	100.1/126.8	501.2

[a] IR intensities (km/mol) are listed in parentheses. [b] Binding energy for the nth Ar ligand.

a barrier of 53 cm^{-1}. Because the low barriers of the H_2O-Ar PES are comparable to the rotational constants of H_2O, this complex is only a slightly hindered internal rotor. In contrast, the PES of the positively charged dimer features a strongly directional H-bond with large barriers to internal rotation. From the rather different binding energies of H_2O^+-Ar (D_e = 2484 cm^{-1}) and H_2O-Ar ($D_e \sim 130$ cm^{-1}) it can be concluded that dispersion provides only a minor contribution to the interaction in the charged dimer.

C. Trimer (n = 2). The trimer equilibrium structure calculated at the MP2 level has the expected planar configuration with two equivalent H-bonds (Figure 1f, C_{2v} symmetry). The properties of this structure are listed in Tables 9 and 10. Owing to noncooperative three-body interactions, the intermolecular H-bonds in the trimer are significantly weaker and longer than in the dimer (D_e = 2067 vs 2484 cm^{-1}, D_0 = 1825 vs 2195 cm^{-1}, R_e = 1.9676 vs 1.9154 Å, MP2). As a consequence of the smaller monomer perturbation, the O−H bonds in the trimer are shorter than the bound O−H_b bond in the dimer (r_e = 1.0161 vs 1.0269 Å). However, they are still significantly longer than in the monomer (r_e = 0.9980 Å). The origin of the noncooperative three-body effect is rationalized in the following way. Complexation of H_2O^+ with the first Ar ligand leads to a substantial elongation of the bound O−H_b bond. The dimer can lower its energy further by simultaneously contracting the free O−H_a bond. Formation of the second H-bond, however, also forces a strong elongation of the O−H_a bond, which in turn leads to contraction of the O−H_b bond compared with the dimer. Thus, both O−H bonds in the trimer are shorter and stronger than the bound O−H_b bond of the dimer leading to weaker intermolecular bonds. Additional three-body contributions arise from the repulsive interaction of the dipole moments induced in the two Ar ligands by the charge distribution of H_2O^+.[1]

The structural effects upon sequential complexation are also reflected in the vibrational frequencies (Table 10). Similar to the monomer, the O−H stretch modes are symmetric and antisymmetric linear combinations of the two equivalent O−H local modes; however, their frequencies are largely red-shifted by complexation compared with free H_2O^+ ($\Delta\nu_1 = -303.3$ cm^{-1}, $\Delta\nu_3 = -410.1$ cm^{-1}, MP2). On the other hand, the shifts are smaller than for the donor stretch in the dimer ($\Delta\nu_1 = -476.6$ cm^{-1}). The ν_2 frequency is nearly unaffected upon sequential complexation. The six intermolecular modes of the trimer can be classified into two stretching and four bending vibrations. The stretching modes are symmetric and antisymmetric combinations of the two intermolecular H−Ar stretch oscillators, $\nu_s(a_1)$ and $\nu_s(b_2)$. The $\nu_b(a_1)$ mode arises from symmetric in-plane bending of the two Ar ligands, whereas the other three bending modes arise from hindered internal rotations of H_2O^+ around its a-, b-, and c-axes, $\nu_b(b_1,a_2,b_2)$. The average ν_s frequency decreases from the dimer to the trimer (207.4 vs 186.5 cm^{-1}) because of weaker intermolecular bonds in the latter complex. In contrast, the in-plane bending frequency increases (352.4 vs 479.5 cm^{-1}) because of the additional constraint arising from the second intermolecular bond. The effects of sequential deuteration on frequencies and IR intensities are summarized in Table 10 (B3LYP) and are in line with the trends discussed for the dimer. Interestingly, the relative order of ν_1 and ν_3 is different in $H_2O^+-Ar_2$ and $D_2O^+-Ar_2$.

The local p-bound minimum on the dimer MP2 potential gives rise to speculations about the existence of less stable trimer isomers, for example, structures with either one p-bond and H-bond or with two p-bonds. Both isomers are calculated to be stationary points on the PES of the trimer at the MP2 level (with total binding energies of D_e = 3980 and 3296 cm^{-1} for the two Ar ligands). Clearly, these isomers can readily be distinguished from the global minimum (total binding energy, D_e = 4551 cm^{-1}) by their rather different O−H stretch frequencies. Indeed, there is some experimental evidence for the existence of a weakly bound isomer with one H-bond and one p-bond, apart from the global minimum with two H-bonds.[13]

D. Larger Clusters (n = 3,4). Because IR spectra of $H_2O^+-Ar_n$ have been recorded up to n = 14,[13] calculations are desired also for systems with $n > 2$. However, these have only been feasible at the HF level, which significantly underestimates the intermolecular interaction (calculations at the B3LYP level for $n > 2$ are not meaningful because of the wrong description of the PES in regions away from hydrogen bonding). Nonetheless, the HF results provide a qualitative picture of further solvation and can be compared with experimental data after applying suitable scaling factors. According to the dimer PES, the cluster growth is expected to proceed by attachment of two further Ar atoms at the p-bound sites of the planar $H_2O^+-Ar_2$ trimer, leading to C_s and C_{2v} symmetric structures for n = 3 and 4, respectively. The properties of these structures relevant for comparison with the experimental data are summarized in Table 11 for n = 0−4.

The trends for complexation with the first two Ar atoms at the two H-bound sites of H_2O have been discussed in detail in sections III.B and III.C: the intermolecular bonds lead to a lengthening of the O—H bonds and a reduction of the O—H stretch frequencies going from $n = 0$ to $n = 2$. Attachment of the next two Ar ligands ($n = 3,4$) at opposite sides of the $2p_y$ orbital of oxygen strengthens the O—H bonds again via partial charge transfer from the Ar atoms into that electrophilic orbital, leading to shorter O—H bonds and incremental blue shifts of ν_1 and ν_3. In general, the effects become weaker upon sequential complexation, because the binding energies decrease as the cluster size increases. This is also reflected in the decreasing frequencies for the intermolecular H—Ar stretching modes. The effects of complexation with the third and fourth Ar ligand go in the same direction but they are not additive and weaker for attachment of the fourth ligand. As a result of the partial charge transfer from the third Ar, the electrophilic character of the $2p_y$ orbital is reduced leading to the weaker interaction with the fourth ligand (which cannot transfer as much charge as the third ligand).

Acknowledgment. This study is part of project 20-055285.98 of the Swiss National Science Foundation. Part of the calculations presented in this paper have been performed using the facilities of the Centro Svizzero di Calcolo Scientifico, Manno, Switzerland.

References and Notes

(1) Nizkorodov, S. A.; Dopfer, O.; Ruchti, T.; Meuwly, M.; Maier, J. P.; Bieske, E. J. *J. Phys. Chem.* **1995**, *99*, 17118.
(2) Dopfer, O.; Olkhov, R. V.; Maier, J. P. *J. Phys. Chem. A* **1999**, *103*, 2982.
(3) Nizkorodov, S. A.; Spinelli, Y.; Bieske, E. J.; Maier, J. P.; Dopfer, O. *Chem. Phys. Lett.* **1997**, *265*, 303.
(4) Olkhov, R. V.; Nizkorodov, S. A.; Dopfer, O. *Chem. Phys.* **1998**, *239*, 393.
(5) Olkhov, R. V.; Nizkorodov, S. A.; Dopfer, O. *J. Chem. Phys.* **1998**, *108*, 10046.
(6) Dopfer, O.; Nizkorodov, S. A.; Meuwly, M.; Bieske, E. J.; Maier, J. P. *Int. J. Mass Spectrom. Ion Processes* **1997**, *167*−*168*, 637.
(7) Lakin, N. M.; Dopfer, O.; Meuwly, M.; Howard, B. J.; Maier, J. P. *Mol. Phys.* **2000**, *98*, 63.
(8) Lakin, N. M.; Dopfer, O.; Howard, B. J.; Maier, J. P. *Mol. Phys.* **2000**, *98*, 81.
(9) Castleman, A. W.; Keesee, R. G. *Chem. Rev.* **1986**, *86*, 589.
(10) Bieske, E. J.; Maier, J. P. *Chem. Rev.* **1993**, *93*, 2603.
(11) Müller-Dethlefs, K.; Dopfer, O.; Wright, T. G. *Chem. Rev.* **1994**, *94*, 1845.
(12) Bieske, E. J.; Dopfer, O. *Chem. Rev.* **2000**, *100*, 3963.
(13) Dopfer, O.; Roth, D.; Maier, J. P. *J. Phys. Chem. A* **2000**, *104*, 11702.
(14) Lopez, G. E. *J. Comp. Chem.* **1995**, *16*, 768.
(15) Bunker, P. R. *Molecular Symmetry and Spectroscopy*; Academic Press: New York, 1979.
(16) Dopfer, O.; Nizkorodov, S. A.; Olkhov, R. V.; Maier, J. P.; Harada, K. *J. Phys. Chem. A* **1998**, *102*, 10017.
(17) Dopfer, O.; Olkhov, R. V.; Roth, D.; Maier, J. P. *Chem. Phys. Lett.* **1998**, *296*, 585.
(18) Dopfer, O.; Roth, D.; Maier, J. P. *J. Chem. Phys.* **2000**, *113*, 120.
(19) Vaidyanathan, G.; Coolbaugh, M. T.; Peifer, W. R.; Garvey, J. F. *J. Phys. Chem.* **1991**, *95*, 4193.
(20) Tuma, C.; Boese, A. D.; Handy, N. C. *Phys. Chem. Chem. Phys.* **1999**, *1*, 3939.
(21) Ruiz, E.; Salahub, D. R.; Vela, A. *J. Am. Chem. Soc.* **1995**, *117*, 1141.
(22) Frisch, M. J. et al. *Gaussian 94*, Revision B.2./E.2.; Gaussian, Inc.: Pittsburgh, PA, 1995.
(23) Frisch, M. J. et al.; *Gaussian 98*, Revision A.5.; Gaussian, Inc.; Pittsburgh, PA, 1998.
(24) Extensible Computational Chemistry Environmental Basis Set Database, version 10, 1996.
(25) Boys, S. F.; Bernardi, F. *Mol. Phys.* **1970**, *19*, 553.
(26) Duijneveldt, V. In *Molecular Interactions*; Scheiner, S., Ed.; Wiley: New York, 1997.
(27) Chalasinski, G.; Szczesniak, M. M. *Chem. Rev.* **1994**, *94*, 1.
(28) Lew, H. *Can. J. Phys.* **1976**, *54*, 2028.
(29) Reutt, J. E.; Wang, L. S.; Lee, Y. T.; Shirley, D. A. *J. Chem. Phys.* **1986**, *85*, 6928.
(30) Dinelli, B. M.; Crofton, M. W.; Oka, T. *J. Mol. Spectrosc.* **1988**, *127*, 1.
(31) Brown, P. R.; Davies, P. B.; Stickland, R. J. *J. Chem. Phys.* **1989**, *91*, 3384.
(32) Huet, T. R.; Pursell, C. J.; Ho, W. C.; Dinelli, B. M.; Oka, T. *J. Chem. Phys.* **1992**, *97*, 5977.
(33) Zajfman, D.; Belacem, A.; Graber, T.; Kanter, E. P.; Mitchell, R. E.; Naaman, R.; Vager, Z.; Zabransky, B. J. *J. Chem. Phys.* **1991**, *94*, 2543.
(34) Forney, D.; Jacox, M. E.; Thompson, W. E. *J. Chem. Phys.* **1993**, *98*, 841.
(35) Botschwina, P. Habilitation thesis, University of Kaiserslautern, 1984.
(36) Botschwina, P. In *Ion and Cluster Ion Spectroscopy and Structure*; Maier, J. P., Ed.; Elsevier: Amsterdam, 1989.
(37) Degli Esposti, A.; Lister, D. G.; Palmieri, P.; Degli Esposti, C. *J. Chem. Phys.* **1987**, *87*, 6772.
(38) Weis, B.; Carter, S.; Rosmus, P.; Werner, H. J.; Knowles, P. J. *J. Chem. Phys.* **1989**, *91*, 2818.
(39) Weis, B.; Yamashita, K. *J. Chem. Phys.* **1993**, *99*, 9512.
(40) Brommer, M.; Weis, B.; Follmeg, B.; Rosmus, P.; Carter, S.; Handy, N. C.; Werner, H. J.; Knowles, P. J. *J. Chem. Phys.* **1993**, *98*, 5222.
(41) Cioslowski, J.; Hay, P. J.; Ritchie, J. P. *J. Phys. Chem.* **1990**, *94*, 148.
(42) Vinograd, S. N.; Linnell, R. H. *Hydrogen Bonding*; Van Nostrand: New York, 1971.
(43) Olkhov, R. V.; Dopfer, O. *Chem. Phys. Lett.* **1999**, *314*, 215.
(44) Herzberg, G. *Molecular Spectra and Molecular Structure. II. Infrared and Raman Spectra of Polyatomic Molecules*; Krieger: Malabar, FL, 1991.
(45) Dopfer, O. et al., unpublished results.
(46) Roth, D.; Nizkorodov, S. A.; Maier, J. P.; Dopfer, O. *J. Chem. Phys.* **1998**, *109*, 3841.
(47) Nizkorodov, S. A.; Roth, D.; Olkhov, R. V.; Maier, J. P.; Dopfer, O. *Chem. Phys. Lett.* **1997**, *278*, 26.
(48) Dopfer, O.; Roth, D.; Maier, J. P. *Chem. Phys. Lett.* **1999**, *310*, 201.
(49) Chalasinski, G.; Klos, J.; Cybulski, M.; Szczesniak, M. *Collect. Czech. Chem. Commun.* **1998**, *63*, 1473.
(50) Hunter, E. P. L.; Lias, S. G. *J. Phys. Chem. Ref. Data* **1998**, *27*, 413.
(51) Tao, F.-M.; Klemperer, W. *J. Chem. Phys.* **1994**, *101*, 1129.
(52) Cohen, R. C.; Saykally, R. J. *J. Chem. Phys.* **1993**, *98*, 6007.